

Article

An Experimental and Theoretical Study of Dye Properties of Thiophenyl Derivatives of 2-Hydroxy-1,4-naphthoquinone (Lawson)

Matías Monroy-Cárdenas ¹, Oscar Forero-Doria ², Ramiro Araya-Maturana ^{1,*} 
and Maximiliano Martínez-Cifuentes ^{3,*} 

¹ Instituto de Química de Recursos Naturales, Universidad de Talca, Talca 3460000, Chile; matias.monroy@utalca.cl

² Departamento de Ciencias Básicas, Facultad de Ciencias, Universidad Santo Tomás, Talca 3460000, Chile; oforero@santotomas.cl

³ Departamento de Química Orgánica, Facultad de Ciencias Químicas, Universidad de Concepción, Edmundo Larenas 129, Concepción 4070371, Chile

* Correspondence: raraya@utalca.cl (R.A.-M.); maxmartinez@udec.cl (M.M.-C.)

Abstract: A prospective study of the dye properties of non-toxic lawson thiophenyl derivatives, obtained using a green synthetic methodology allowed for the description of their bathochromic shifts in comparison to those of lawson, a well-known natural pigment used as a colorant that recently also has aroused interest in dye-sensitized solar cells (DSSCs). These compounds exhibited colors close to red, with absorption bands in visible and UV wavelength range. The colorimetric study showed that these compounds exhibited a darker color than that of lawson within a range of colors depending on the substituent in the phenyl ring. Computational calculations employing Density Functional Theory (DFT) and Time-Dependent Density Functional Theory (TD-DFT), showed that the derivatives have lower excitation energies than lawson, while the alignment of their frontier orbitals regarding the conduction bands of TiO₂ and ZnO and the redox potential of the electrolyte I⁻/I₃⁻ suggests that they could be employed as sensitizers. The study of the interactions of the lawson and a derivative with a TiO₂ surface model by different anchoring modes, showed that the adsorption is thermodynamically favored. Natural bond orbital (NBO) analysis indicates a two-center bonding (BD) O-Ti as the main interaction of the dyes with TiO₂.

Keywords: lawson derivatives; dye-sensitized solar cells; metal-free organic dyes; photovoltaic parameters



Citation: Monroy-Cárdenas, M.; Forero-Doria, O.; Araya-Maturana, R.; Martínez-Cifuentes, M. An Experimental and Theoretical Study of Dye Properties of Thiophenyl Derivatives of 2-Hydroxy-1,4-naphthoquinone (Lawson). *Materials* **2021**, *14*, 5587. <https://doi.org/10.3390/ma14195587>

Academic Editors: Marcin Jasiński, Adam Marek Pieczonka and Grzegorz Młostko

Received: 29 July 2021

Accepted: 23 September 2021

Published: 26 September 2021

Publisher's Note: MDPI stays neutral with regard to jurisdictional claims in published maps and institutional affiliations.



Copyright: © 2021 by the authors. Licensee MDPI, Basel, Switzerland. This article is an open access article distributed under the terms and conditions of the Creative Commons Attribution (CC BY) license (<https://creativecommons.org/licenses/by/4.0/>).

1. Introduction

Since the components of the quinone/hydroquinone redox couple are easily interconvertible and closely balanced energetically [1,2], they serve as important links in electron transport processes during metabolic pathways and many biological reactions [3], also explaining their use in industrial applications [4–7]. Among naturally occurring quinones, lawson (2-hydroxy-1,4-naphthoquinone), a red-orange pigment, present in henna, has long been used for the coloration of the skin, hair, and textile materials [8]. Important reasons for the use of lawson as a dye are the ease of obtaining it and the absence of environmental problems related to its use. It has been demonstrated to not be mutagenic in catalase mutant *Escherichia coli*, both in the absence and presence of metabolic activation [9]. On the other hand, it has been suggested that its low cytotoxicity is probably mediated, at least in part, by the release of reactive oxygen species [9]. However, extensive research in the field of synthetic dyestuffs has led to a drastic decline in the use of natural dyes because of their limited range of colors among other disadvantages. Despite the advantages that synthetic compounds offer in this area, several synthetic colorants are ultimately environmentally deleterious. On the other hand, besides its use as a textile colorant, lawson has aroused a recent interest in the fields of protein crystallography [10] and dye-sensitized solar cells

(DSSCs). In DSSCs, it has been employed as a dye sensitizer (which acts as both a light absorber and electron donor) [11], where it is attached to a semiconductor anode surface, which consists of an inorganic mesoporous oxide layer acting as electron acceptor. When sunlight is absorbed by the dye, an ultrafast electron transfer from the dye's first excited state to the conduction band states of the semiconductor occurs. Then, the oxidized dye is neutralized by the reduced form of a redox mediator, which can be either a liquid electrolyte redox couple (usually iodide/triiodide or metal complexes) or a solid-state positive charge (hole) transporter. Finally, the oxidized redox mediator is neutralized at the cathode to close the circuit. A major requirement of an efficient solar cell sensitizer is to have an extended UV/Vis absorption spectrum closely matching that of solar radiation [12]. In this way, the dye sensitizer plays an essential role in achieving a high-power conversion efficiency of the DSSC [12]. The development of dye sensitizer can be grouped in two main sets: (a) dyes based on the ruthenium (II) complex and (b) metal-free organic donor–acceptor dyes [13]. The first group contains the metal ruthenium, which has a high environmental impact and is expensive. The second group of dyes presents major advantages due to their inexpensive cost and tunable molecular design [13]. It is important to note that among the second group, natural pigments as sensitizers have emerged as an interesting option [14–20]. One of the main ways by which higher power conversion efficiency in DSSCs can be achieved is the development of a sensitizer capable of using photons from the near-infrared spectral region [21]. Some studies on the performance of lawsone in DSSCs indicated the energy conversion efficiency to be 0.93% with an absorption spectrum range of 200–410 nm. Moreover, co-sensitization with lawsone has been used to improve the performance of betanin solar cells [22,23]. Although the above shows that lawsone represents a promising prospect, it is important to identify derivatives that have a wider absorption range at wavelengths closer to the near-infrared spectral region.

Lawsone and its conjugated base are involved in a pH-dependent equilibrium. The acidic solution of lawsone is colorless, although, with increased pH values, an absorption maximum of around 450 nm develops, and this gives rise to the characteristic orange color. The solution in acetonitrile is very pale yellow and presents an absorption band at 333 nm, but it turns intense yellow upon dilution with water. However, the absorptions of the UV/Vis spectrum of lawsone in dimethyl sulfoxide are observed at the 296, 339, 416, and 448 nm wavelengths [24].

There are few examples in the literature regarding the tuneability of the spectroscopy properties of lawsone using structural modifications. One example is the tuning of the original color of lawsone using cocrystallization with pyridine derivatives [25].

Thus, this study aims to assess the impact of structural modifications on dye characteristics. Lawsone thiophenyl derivatives are easily accessible via a green synthetic methodology and have shown low toxicity in a previous study [26]. An experimental–theoretical approach was used to carry out a detailed description of the properties of these derivatives as dyes (Table 1), and the potential application in colorimetry and solar cells compared with that of lawsone is discussed.

Table 1. Compounds studied in this work [26].

Cpd	1	2	3	4	5	6	7	8	9
X	Lawsone	H	<i>o</i> -CO ₂ Me	<i>o</i> -Br	<i>m</i> -Br	<i>p</i> -Br	<i>o</i> -F	<i>m</i> -Br	<i>p</i> -Br

The reaction scheme shows the synthesis of thiophenyl lawsone derivatives. On the left, Lawsone (1) is shown as a naphthalene ring with two carbonyl groups and a hydroxyl group at the 1-position. It reacts with a thiophenyl derivative (2) which has a thiol group (-SH) at the 2-position and a substituent X at the 5-position. The reaction is carried out 'on water'. The products are a thiophenyl lawsone derivative (3-9) where the thiophenyl group is attached to the 3-position of the naphthalene ring, and a hydroquinone derivative (4-9) where the hydroxyl group is at the 1-position and the substituent X is at the 4-position of the benzene ring.

2. Results

2.1. Colorimetric Study

The CIE Lab system was used to evaluate the color parameters and the color differences of the thiophenyl derivatives of lawsone; the results are shown in Table 2. According to a^* and b^* values, their colors were present in the yellow-red quadrant. These compounds showed L^* values < 40 , indicating that they have darker colors than those of lawsone (1) ($L^* > 60$). The color differences (ΔE) were significant at 51.8–71.2 (Figure 1) due to the incorporation of the differently substituted thiophenyl moieties in lawsone structure 1. The bromo derivatives, such as 5 and 6, showed the highest ΔE with values of 71.2 and 70.4, respectively, while fluoro derivatives 7 and 9 showed the lowest values of 65.6 and 67.4, respectively. The L^* value of 1 was compared with the published value of the henna dye solution [27].

Table 2. Colorimetric properties of thio derivatives of lawsone.

Compound	L^*	a^*	b^*	c^*	h°	ΔE
1	65.01	1.76	51.64	51.67	88.04	-
2	18.70	17.15	3.50	17.50	11.55	69.1
3	30.30	33.78	25.39	42.26	36.93	54.1
4	36.62	19.29	12.96	23.24	33.90	51.8
5	15.19	9.52	1.95	9.71	11.56	71.2
6	21.34	11.22	-3.34	11.70	343.41	70.4
7	31.12	4.69	-5.40	7.15	310.97	65.6
8	27.90	31.58	19.31	37.24	31.23	58.0
9	17.07	6.38	4.71	7.93	36.42	67.4

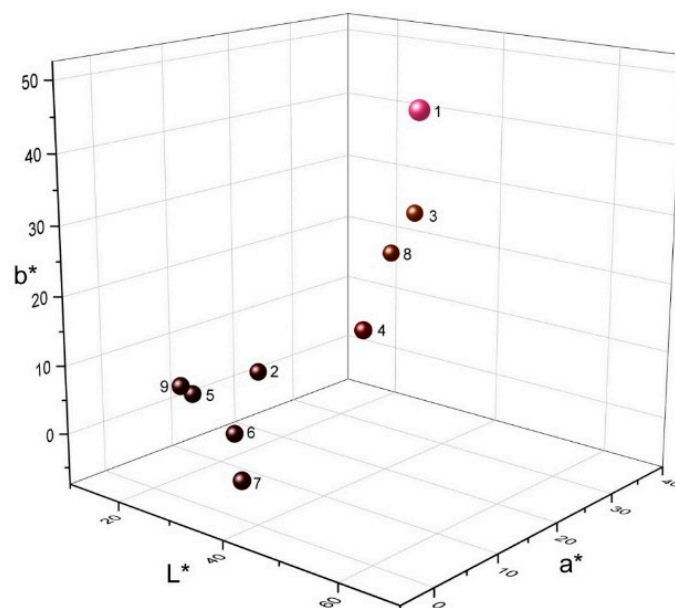


Figure 1. Three-dimensional chromaticity diagram of the different thio-lawsone derivatives.

Lawsone analogs, such as the natural anthraquinones emodin and dermocybin, exhibit differences in color; i.e., emodin dyed polyamide is brownish-orange, while dyed with dermocybin is wine red, but on polyester, the colors are totally different: bright yellow and bright reddish-orange, respectively [28]. Similar results were obtained for different styryl and azo-lawsone dyes of synthetic origin, exhibiting brown (CIELab: 25.057, 13.577, and 17.516) and orange (CIELab: 63.554, 36.699, and 67.159) colors on polyester, respectively, while on nylon, both exhibited darker colors ($L^* < 40$) in the yellow-red quadrant, which agree with our results [29,30]. Moreover, polymers based on lawsone have been obtained with color differences. For example, Mahkam et al. (2014) synthesized a series of polymers derived from lawsone with acryloyl chloride, methacrylic acid, acrylic acid,

and acrylonitrile to obtain different polymers using free-radical copolymerization. The resulting polymers presented colors in the yellow-red quadrant [31] in a similar manner to the thiophenyl lawsone derivatives reported here.

Generally, the color of dyes depends on the nature of their coupled components [32]; consequently, this series of lawsone derivatives shows that it is possible to obtain a wide gamma of colors by replacing the substituent in the phenyl ring of this kind of lawsone thiophenyl derivative, thereby suggesting potential industrial uses.

2.2. UV/Vis Spectroscopy

Figure 2 and Table 3 resume experimental UV/Vis results. Figure 2 shows the absorption bands from 200 to 700 nm for lawsone and its thiophenyl derivatives 2 and 3 (spectra for all compounds are presented in supporting information). Lawsone dyes exhibited peaks at range 208–334 nm. The band at 334 nm is attributed to C=O and OH groups [33], and its long tail in the visible region is responsible for the yellow-orange color of lawsone [34].

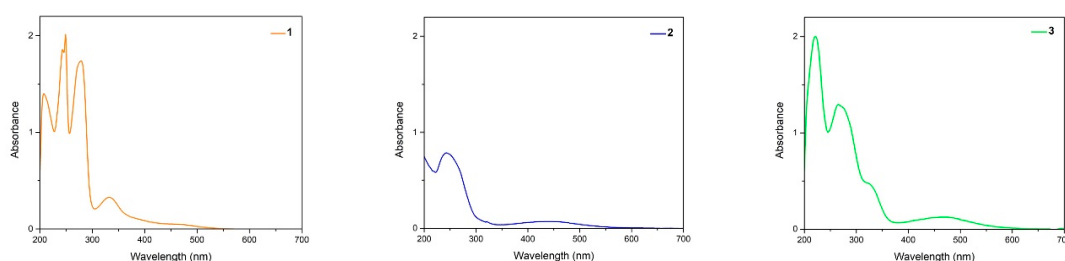


Figure 2. UV/Vis absorption spectra of compounds 1, 2, and 3 in methanol. Spectra for all compounds are presented in supporting information.

Table 3. Experimental UV/Vis spectrum in methanol.

	Thio-Lawsone Derivatives								
	1	2	3	4	5	6	7	8	9
λ exp (nm)	208	270	222	213	212	207	208	208	205
	243	459	268	267	266	264	251	210	265
	249		273	465	467	478	280	252	277
	279		325				463	279	473
	334		474					465	

UV/Vis spectra of lawsone derivatives showed bands at range 205–478 nm. The latter indicates a bathochromic shift from 334 nm (lawsone) to values over 450 nm. This displacement to the visible region corresponds with a color close to red for all derivatives.

2.3. Theoretical Calculations

2.3.1. Electronic and Spectroscopic Study

To gain insight into the molecular structure and the effect of modifications on the electron distribution and energy levels of lawsone derivatives, we carried out DFT and TD-DFT calculations. To evaluate different functionals and their suitability to this kind of calculation, we chose three DFT functionals, B3LYP, M06-2X, and HSE2PBE, in addition to the 6-311+G(d,p) basis set to perform the calculations. To evaluate the accuracy of the employed functionals, we compared the HOMO energy of lawsone obtained experimentally [35] with values obtained using these functionals. The calculated EHOMO was -7.50 eV for HSE2PBE, -8.80 eV for M06-2x, and -7.36 eV for B3LYP. B3LYP gave a value closer to the experimentally reported value (-5.21 eV) than the other functionals did. Therefore, we continue our study with the results obtained when using this function.

The optimized geometries, as well as HOMO and LUMO distribution for lawsone and its thio derivatives, are presented in Figure 3.

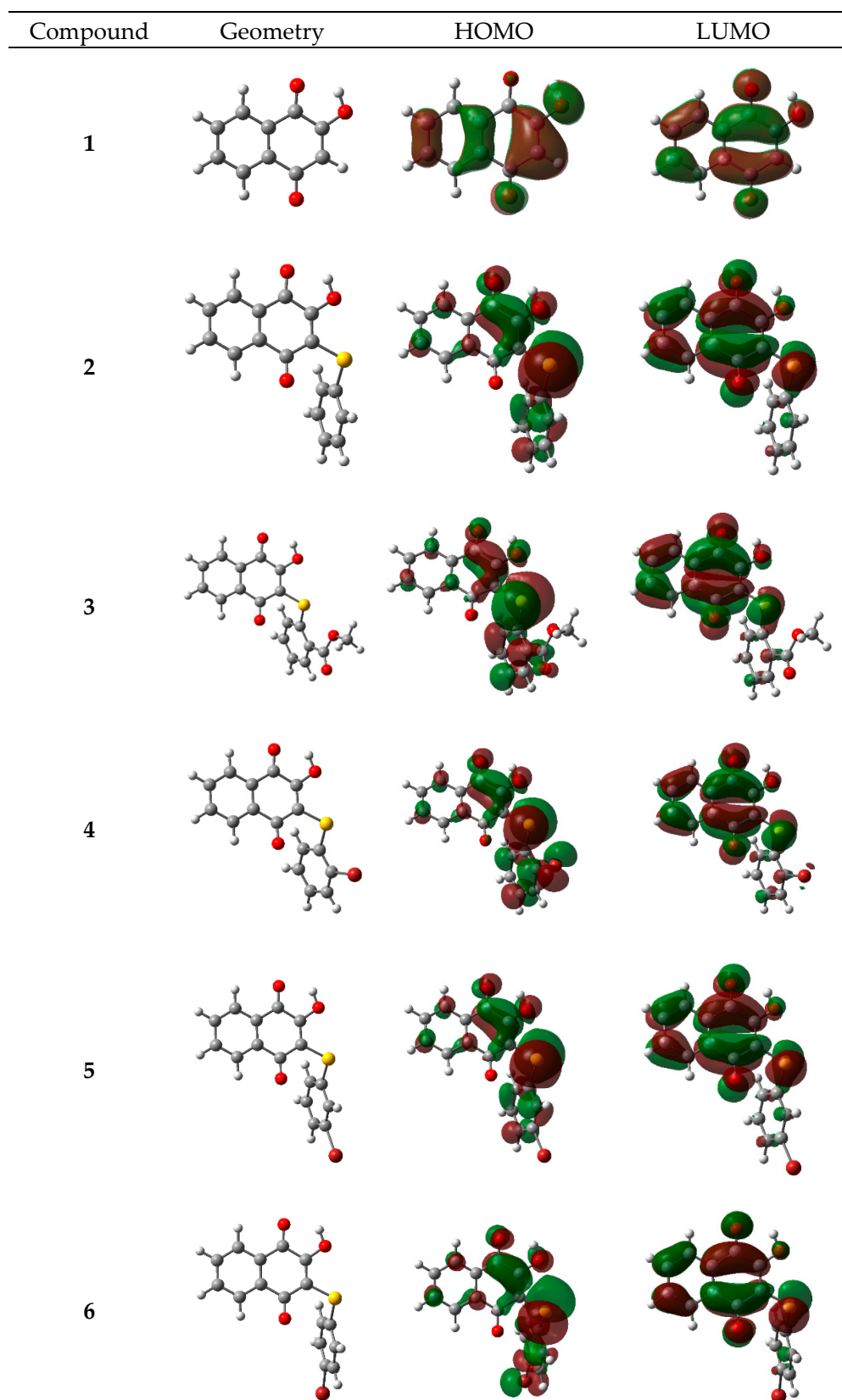


Figure 3. Cont.

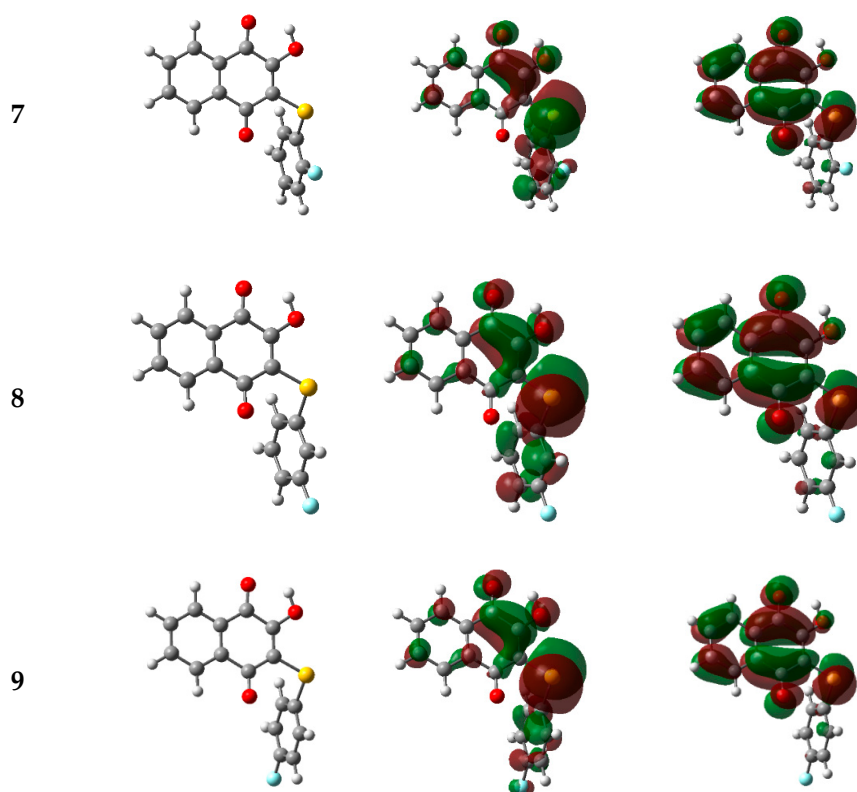


Figure 3. Optimized geometries and electronic densities corresponding to the HOMO and LUMO energy levels for all studied molecules.

All derivatives present a CSC angle at about 103° , and dihedral CCSC at about 50° , which leads to the formation of the aromatic ring of thiophenyl moiety, and the quinonic ring does not become coplanar. This structural feature can lead to a decline in the charge transfer between both sides of the molecule and also generates an anti-aggregation effect [36]. It has been widely studied that aggregation of dyes that can interact by π - π interactions tend to negatively affect their performance in DSSCs [37]. Aggregation of dyes molecules in a face-to-face alignment, as occur in p-p interactions, lead to hypsochromic absorption shift (H-aggregate) [37]. The latter avoids that dye can absorb in the longer-wavelength region of the visible and near-infra-red (NIR) spectrum, which are a desirable part of the spectrum. It has been experimentally tested that for organic dyes, aggregation, when they are on TiO_2 surface leads to quenching of the excited states of the dyes, resulting in low efficiency of electron injection [38,39]. Besides, aggregation favor charge recombination between the injected electrons in the semiconductor and the oxidized redox mediator in the electrolyte resulting in a reduced V_{oc} value [39–41].

In the case of lawsone, its coplanarity favors their potential aggregation by π - π interactions. Therefore, non-planar derivatives which prevent this kind of aggregation can lead to an improvement in their dye sensitizer performance [42].

Electronic distribution of frontier orbitals demonstrates that for all derivatives, the HOMO is localized mainly on the thiophenyl moiety and partially spread on the quinone ring. On the other hand, also for all derivatives, LUMO is fully localized on the quinone ring and sulfur atom with almost no presence on the aromatic ring of the thiophenyl moiety. These results show that overlap between HOMO and LUMO occurs in the lower extension for these derivatives when compared with that for lawsone.

To understand the experimental UV/Vis results, TD-DFT calculations were carried out for all compounds. Table 4 presents the excitation energies (E_{ex}), wavelength (λ), oscillator strengths (f), light-harvesting efficiency (LHE), and the corresponding electronic transition for selected relevant excited state (full data is in Table S1 of SI). As has been previously de-

scribed for lawsone, the most probable transitions, in both vacuum and solution (methanol), fall in the UV region, and they occur from the ground state to excited states 4 and 5, which can be assigned mostly to the H-2→L and H-3→L MOs [14]. On the other hand, for all these derivatives, the most probable transitions, in both vacuum and solution (methanol), fall in both the visible and UV regions; occur from the ground state to excited states 1 and 8 (7 for Cpd 3), respectively; and can be assigned mostly to the H→L and H→L+1 MOs. The LHEs calculated for lawsone in vacuum are similar to those previously described [14], and they are considered rather low, as in the general case of natural dyes [43,44]. In methanol, we noted that LHE increased more than in dimethyl sulfoxide and dichloromethane according to a previous report [14]. LHEs for thiophenyl derivatives of lawsone decrease slightly, but they demonstrate absorption in the visible range, which benefits their potential performance in DSSCs. Comparisons among theoretical and experimental UV peaks are shown in Table S2 of the Supplementary Material.

Table 4. Excitation energies (E_{ex}), wavelength (λ), oscillator strengths (f), light-harvesting efficiency (LHE), and the corresponding electronic transition for each relevant excited state.

Excited State N°.	Vacuum					Methanol					
	E_{ex} , eV	λ , nm	f	LHE	Electronic Transition	Excited State No.	E_{ex} , eV	λ , nm	f	LHE	Electronic Transition
Cpd 1						Cpd 1					
ES 4	3.69	336	0.058	0.125	H-2→L (91%)	4	3.57	348	0.075	0.159	H-2→L (47%)
ES 5	4.31	288	0.177	0.334	H-3→L (88%)	5	3.20	295	0.249	0.436	H-3→L (92%)
Cpd 2						Cpd 2					
ES 1	2.11	587	0.052	0.112	H→L (98%)	1	2.20	562	0.059	0.127	H→L (98%)
ES 8	3.93	315	0.172	0.327	H→L+1 (88%)	8	4.13	300	0.205	0.376	H→L+1 (96%)
Cpd 3						Cpd 3					
ES 1	1.99	624	0.053	0.114	H→L (99%)	1	2.15	577	0.059	0.127	H→L (99%)
ES 7	3.79	327	0.196	0.364	H→L+1 (77%)	7	3.90	318	0.201	0.370	H→L+1 (96%)

To study the alignment of energy levels, which define the overall conversion efficiency of DSSCs, we considered the alignment of the frontier MOs energy levels of the compounds with valence and a conduction band edge of the semiconductors TiO₂ and ZnO. Table 5 lists the MOs, excitation energies E_{ex} , energy gaps E_{gap} , and excited-state oxidation potentials (ESOPs). ESOPs have been proposed as appropriate for the representation of excited states, and they were calculated from occupied energy levels and relevant excitation energies [14,45,46]. E_{ex} is the most important factor in the evaluation of the efficiency of DSSCs, as a sensitizer with a low E_{ex} facilitates light absorption in the long-wavelength range [14]. We noted that thiophenol derivatives present lower E_{ex} than lawsone, which indicates that they could be better sensitizers.

Energy diagrams of the most relevant MOs of the species in both the gas phase and solution are shown in Figure 4. E_{LUMO} of a good photosensitizer dye should lie slightly above the conduction band (CB) edge of the semiconductor to ensure electron injection from the excited dye [47], while E_{HOMO} should lie under the redox potential of the electrolyte for dye regeneration by accepting electrons from the electrolyte [23]. We used a TiO₂ (CB = −4.05 eV [48]) ZnO (CB = −4.45 [49]) semiconductor in addition to the electrolyte I[−]/I₃[−] (−4.80 eV [50]) to evaluate our compounds. As displayed in Figure 4, all thiophenyl derivatives of lawsone meet the criteria of energy level alignment to be appropriate photosensitizers for TiO₂ and ZnO semiconductors. In the case of TiO₂, the gap between CB and E_{LUMO} is lower than that for ZnO, which suggests that these compounds perform well as sensitizers in DSSC with TiO₂. Besides, E_{HOMO} for all derivatives lie below the redox level of the I[−]/I₃[−] electrolyte, allowing electron transfer to the dye from the electrolyte.

Table 5. Energies of molecular orbitals, excitation energies E_{ex} , energy gaps E_g , and excited-state oxidation potentials (ESOPs) for each relevant transition.

Vacuum						Methanol					
MO	E_{MO} eV	Transition	E_{ex}	E_g	ESOP	MO	E_{MO} eV	Transition	E_{ex}	E_g	ESOP
Cpd 1						Cpd 1					
H-3	-8.13	H-3→L	4.31	4.54	-3.83	H-3	-8.04	H-3→L	3.20	4.48	-4.84
H-2	-7.87	H-2→L	3.69	4.28	-4.18	H-2	-7.76	H-2→L	3.57	4.20	-4.19
H	-7.4	H→L	3.13	3.81	-4.27	H	-7.36	H→L	3.06	3.80	-4.30
L	-3.59					L	-3.56				
L + 1	-1.76					L + 1	-1.64				
Cpd 2						Cpd 2					
H-4	-7.84	H-4→L	3.67	4.31	-4.17	H-3	-7.74	H-3→L	3.55	4.15	-4.19
H-1	-7.15	H-1→L	2.77	3.62	-4.38	H-1	-7.29	H-1→L	2.88	3.70	-4.41
H	-6.21	H→L	2.11	2.68	-4.10	H	-6.40	H→L	2.20	2.81	-4.20
L	-3.53					L	-3.59				
L + 1	-1.75					L + 1	-1.69				
Cpd 3						Cpd 3					
H-6	-8.11	H-6→L	3.94	4.47	-4.17	H-3	-7.76	H-3→L	3.53	4.12	-4.23
H-5	-7.93	H-5→L	3.65	4.29	-4.28	H-1	-7.51	H-1→L	2.95	3.87	-4.56
H	-6.2	H→L	1.99	2.56	-4.21	H	-6.40	H→L	2.15	2.76	-4.25
L	-3.64					L	-3.64				
L + 1	-1.85					L + 1	-1.83				
Cpd 4						Cpd 4					
H-4	-7.92	H-4→L	3.65	4.27	-4.27	H-3	-7.77	H-3→L	3.53	4.13	-4.24
H-1	-6.95	H-1→L	2.76	3.30	-4.19	H-1	-7.14	H-1→L	2.91	3.50	-4.23
H	-6.22	H→L	2.01	2.57	-4.21	H	-6.40	H→L	2.15	2.76	-4.25
L	-3.65					L	-3.64				
L + 1	-1.86					L + 1	-1.74				
Cpd 5						Cpd 5					
H-4	-7.94	H-4→L	3.66	4.28	-4.28	H-3	-7.76	H-3→L	3.54	4.14	-4.22
H-2	-7.41	H-2→L	2.81	3.75	-4.60	H-2	-7.46	H-2→L	2.91	3.84	-4.55
H	-6.39	H→L	2.15	2.73	-4.24	H	-6.49	H→L	2.25	2.87	-4.24
L	-3.66					L	-3.62				
L + 1	-1.86					L + 1	-1.72				
Cpd 6						Cpd 6					
H-1	-7.12	H-1→L	2.75	3.48	-4.37	H-3	-7.75	H-3→L	3.53	4.14	-4.22
H	-6.33	H→L	2.13	2.69	-4.20	H-1	-7.20	H-1→L	2.85	3.59	-4.35
L	-3.64					H	-6.44	H→L	2.23	2.83	-4.21
L + 1	-1.84					L	-3.61				
						L + 1	-1.71				
Cpd 7						Cpd 7					
H-4	-7.89	H-4→L	3.65	4.29	-4.24	H-3	-7.76	H-3→L	3.54	4.14	-4.22
H-1	-7.11	H-1→L	2.75	3.51	-4.36	H-1	-7.24	H-1→L	2.88	3.62	-4.36
H	-6.31	H→L	2.17	2.71	-4.14	H	-6.48	H→L	2.25	2.86	-4.23
L	-3.6					L	-3.62				
L + 1	-1.8					L + 1	-1.71				
Cpd 8						Cpd 8					
H-4	-7.93	H-4→L	3.66	4.29	-4.27	H-3	-7.76	H-3→L	3.55	4.15	-4.21
H-2	-7.4	H-2→L	2.81	3.76	-4.59	H-2	-7.46	H-2→L	2.92	3.85	-4.54
H	-6.36	H→L	2.15	2.72	-4.21	H	-6.47	H→L	2.25	2.86	-4.22
L	-3.64					L	-3.61				
L + 1	-1.84					L + 1	-1.71				
Cpd 9						Cpd 9					
H-1	-7.17	H-1→L	2.75	3.56	-4.42	H-3	-7.74	H-3→L	3.54	4.15	-4.20
H	-6.37	H→L	2.17	2.76	-4.20	H-1	-7.26	H-1→L	2.84	3.67	-4.42
L	-3.61					H	-6.48	H→L	2.27	2.89	-4.21
L + 1	-1.82					L	-3.59				
						L + 1	-1.69				

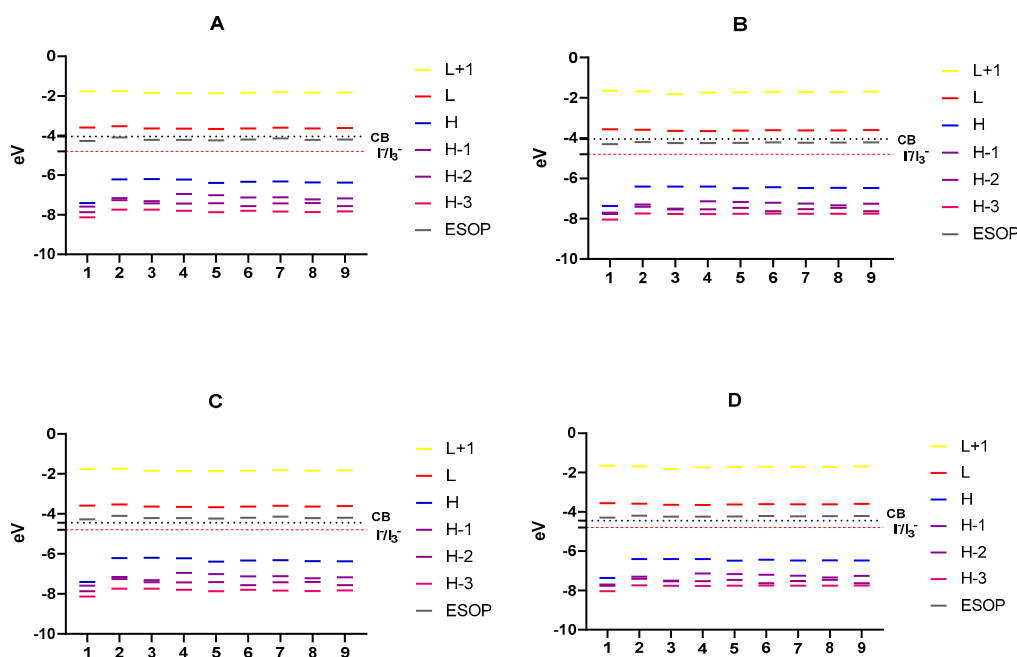


Figure 4. Level alignment of each compound regarding TiO_2 ((A) in vacuum and (B) in methanol) and ZnO ((C) in vacuum and (D) in methanol). Alignment regarding electrolyte I^-/I_3^- is shown in each case. Values for TiO_2 and ZnO have been obtained from references [48,49].

2.3.2. Adsorption of Lawsone and 3-Thiophenyl-lawsone on a TiO_2 Model

An essential requisite for an organic dye can effectively acts as a sensitizer in DSSCs, is the anchoring to the surface of the semiconductor. The latter can be achieved by incorporating different polar functional groups in the structure of sensitizer (as carboxylic acid, amines, ketones, among others). Prinzisky et al. studied the performance of a hydroxy-anthraquinone imine as a dye for DSSCs [51], where the hydroxyl and imine groups acting anchoring the molecule to the TiO_2 semiconductor surface. Recently, Sreeja and Pesala studied the performance of natural dyes indigo, lawsone, and betanin as co-sensitizer for solar cells [23]. They associated one carbonyl group of the lawsone as an anchor group to the surface of TiO_2 . However, lawsone possesses a hydroxyl group in the alpha position to one of the carbonyls of the quinone ring, which can additionally contribute to anchoring the molecule to the surface of the semiconductor. Considering this background, we studied the interactions between lawsone and 3-thiophenyl-lawsone with a TiO_2 surface model by DFT calculations. The adsorption of the dyes was simulated with a $(\text{TiO}_2)_9$ cluster, based on previous works of Sánchez de Armas et al. [52,53], who showed that a group of $(\text{TiO}_2)_9$ is large enough to reproduce adequately the electronic properties of a dye- TiO_2 system. There are different ways to adsorb a dye onto a TiO_2 surface, depending on the conditions used to prepare DSSC [37]. Considering the above, we explored three possible anchoring modes for both molecules, depending on the protonation state of the hydroxyl (Figure 5). The first mode corresponds to a not dissociate state of hydroxyl (neutral I), the second mode corresponds to a dissociate state, where the hydroxyl proton is transferred to an oxygen of TiO_2 surface (neutral II), and the third mode corresponds to a dissociate state where the hydroxyl proton is transferred to another species with basic character, potentially present in the medium (anionic).

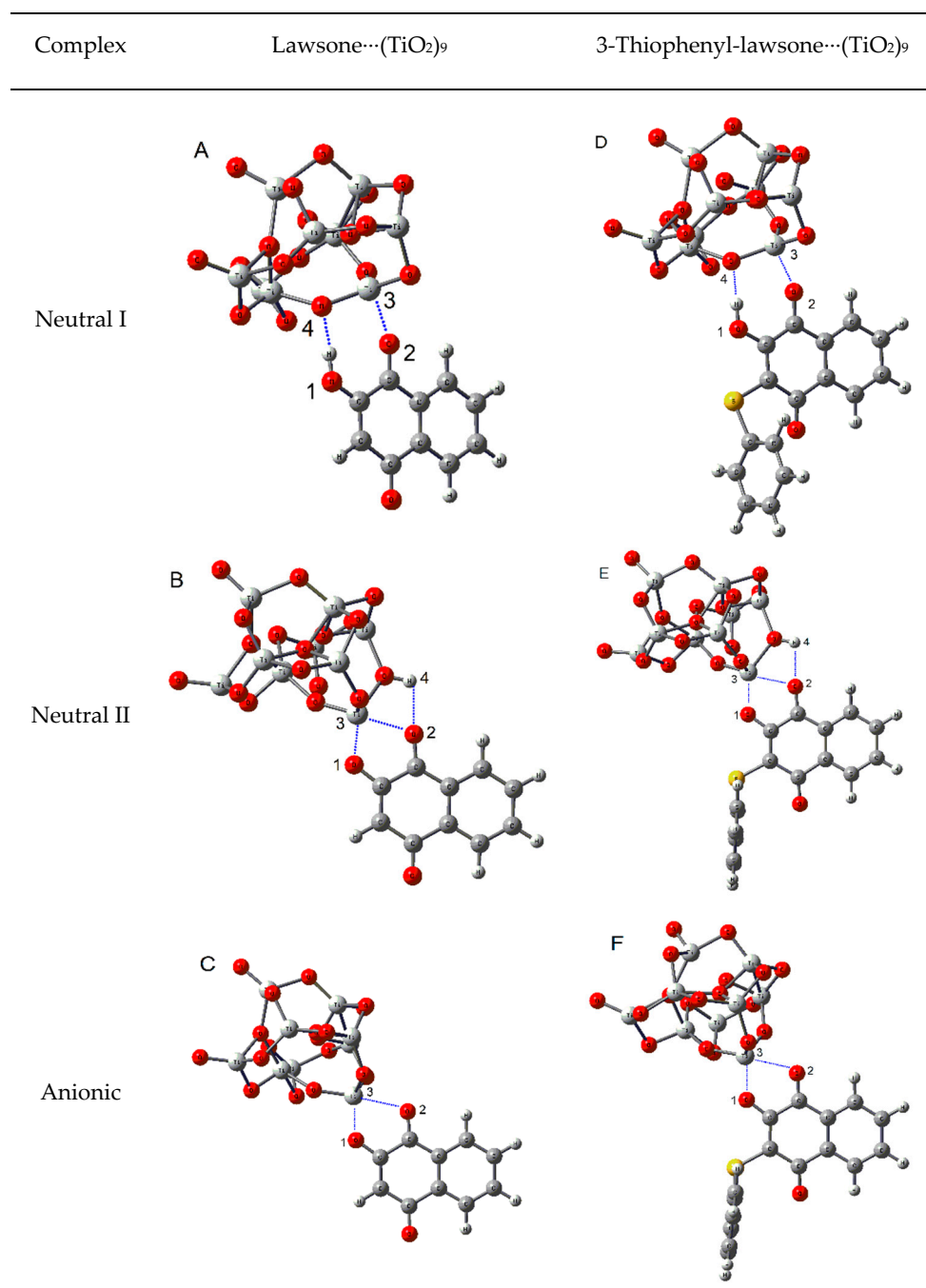


Figure 5. Optimized geometries for the complexes (A) neutral lawsone \cdots (TiO₂)₉, (B) neutral deprotonated lawsone \cdots (TiO₂)₉, (C) anionic deprotonated lawsone \cdots (TiO₂)₉, (D) neutral 3-thiophenyl-lawsone \cdots (TiO₂)₉, (E) neutral deprotonated 3-thiophenyl-lawsone \cdots (TiO₂)₉, and (F) anionic deprotonated 3-thiophenyl-lawsone \cdots (TiO₂)₉. Calculations at B3LYP DFT level with basis set 6-311G(d,p) for C, H, S, and H atoms, and LanL2DZ for Ti atoms.

For the first mode (neutral I), we found that two interactions are responsible for the anchoring: an intermolecular hydrogen bond (IHB) between the -OH in the dye and an oxygen in the TiO₂ cluster, along with an interaction between the oxygen of a carbonyl group. The distance of O1-H1 \cdots O3 was 1.70 Å for both complexes. In the case of O2 \cdots Ti3 interaction, the distance was slightly shorter for the 3-thiophenyl-lawsone \cdots (TiO₂)₉ complex compared to lawsone \cdots (TiO₂)₉ (2.00 vs. 2.03 Å). For the second mode (neutral II), a bidentate interaction between both neighbor oxygen in the dye with one Ti on the surface, along with a potential IHB between oxygen protonated in the cluster and one of the oxy-

gen in the dye, are responsible for the adsorption. The latter mode is similar to it found when carboxylic acid groups binding to TiO₂ surface [54–56]. Distances for intermolecular interactions O1...T3, O2...T3, and O2...H4 were shorter for the complex 3-thiophenyl-lawsone...TiO₂ compared to those for complex lawsone...TiO₂ (1.89 versus 1.92 Å, 2.01 versus 2.28 Å, and 2.02 versus 2.17 Å, respectively). The third mode (Figure 5C,F), with anionic deprotonated species, showed a similar configuration to the second mode, with a Ti of cluster interacting with two neighbor carbonyl in the dyes. For lawsone...TiO₂ complex the O1...T3 distance was shorter compared to those of 3-thiophenyl-lawsone...TiO₂ complex (1.94 versus 2.47 Å, respectively). On the other hand, the O2...T3 distance was shorter 3-thiophenyl-lawsone...TiO₂ compared to those of lawsone...TiO₂ complex (2.43 versus 2.47 Å, respectively).

To evaluate the anchoring of the studied dyes on the TiO₂ surface quantitatively, we calculated the adsorption energies (E_{ads}) for the complexes as follows [57,58]:

$$E_{\text{ads}} = E_{\text{dye-TiO}_2} - E_{\text{dye}} - E_{\text{TiO}_2} \quad (1)$$

where $E_{\text{dye-TiO}_2}$ correspond to the energy of complex, E_{dye} to the energy of the isolated dye, and E_{TiO_2} to the energy of isolated (TiO₂)₉ cluster. Table 6 presents the values of E_{ads} for each complex, as well as their HOMO, LUMO, and gap energies (E_{gap}). All complexes presented negatives E_{ads} , indicating that anchoring of these dyes is thermodynamically favorable. Between the two neutral adsorption mode, the second (bidentate) was more favorable for both dyes. Comparing between lawsone and 3-thiophenyl-lawsone, the latter presents a more negative value, indicating a stronger interaction with the TiO₂ cluster. Anionic complexes present the most negative E_{ads} for both dyes (C and F), indicating that they interacts stronger with TiO₂ cluster than the neutral forms. Unlike the second mode of adsorption (the most favorable between neutrals), lawsone presented a complex more stable than 3-thiophenyl-lawsone. The value of E_{ads} obtained for complexes (−17.79 to −97.39 kcal/mol) indicates in all cases a strong enough interactions that allow one to suggest that these dyes are chemisorbed on the surface of TiO₂ [57,59].

Table 6. Adsorption energies (E_{ads}), HOMO energies (E_{HOMO}), LUMO energies (E_{LUMO}) and gap HOMO-LUMO energies (E_{gap}) for the six complexes A–F.

Complex	E_{HOMO} (eV)	E_{LUMO} (eV)	E_{gap} (eV)	E_{ads} (kcal/mol)
(A) Neutral lawsone...TiO ₂	−7.97	−4.84	3.13	−19.94
(B) Neutral deprotonated lawsone...TiO ₂	−7.74	−4.42	3.32	−44.60
(C) Anionic deprotonated lawsone...TiO ₂	−5.08	−1.61	3.47	−97.39
(D) Neutral 3-thiophenyl-lawsone...TiO ₂	−6.92	−4.68	2.24	−17.79
(E) Neutral deprotonated 3-thiophenyl-lawsone...TiO ₂	−6.62	−4.30	2.32	−46.30
(F) Anionic deprotonated 3-thiophenyl-lawsone...TiO ₂	−4.28	−1.69	2.59	−80.30

To analyze the nature of the interaction between anchoring atoms in the dyes with the atoms on the surface of the TiO₂ cluster, we carried out a natural bond orbital (NBO) analysis for the most stable neutral complexes B and E, and for anionic C and F [60]. The results showed that all complexes studied present a two-center bond of type BD for O1-Ti₃, which explains the strong E_{ads} . The results also showed a less strong donor-acceptor interaction between a LP of O₂ with Ti₃ atoms in the cluster for C and F. Additionally, an interaction LP of O₂ with H4 in the TiO₂ cluster for B and E, which is characteristic of hydrogen bonds [60].

3. Materials and Methods

3.1. Synthesis

Compounds 1–7 were obtained using an on-water methodology previously described [26]. ^1H and ^{13}C NMR spectra were obtained from a spectrometer operating at either 400.13 MHz (^1H) or 100.61 MHz (^{13}C) at 300 K. All melting points were uncorrected and were determined using Electrothermal 9100 apparatus (Cole-Parmer, Stone, UK). Silica gel 60 (230–400 mesh ASTM) and TLC aluminum sheets silica gel 60 F254 were used for flash-column chromatography and analytical TLC, respectively.

3.2. Color Evaluation by Nix Pro Sensor

CIE Lab coordinates (L^* , a^* , b^* , C^* , and h° , where L^* denotes lightness, a the red/green value, b^* the yellow/blue value, C^* the saturation value, and h° is the hue) [45] were calculated from the reflectance data of the 10° observer and daylight.

The color differences between the derivatives of lawsone and lawsone were calculated as follows:

$$\Delta E = \sqrt{(\Delta L^*)^2 + (\Delta a^*)^2 + (\Delta b^*)^2} \quad (2)$$

3.3. Measurement of the UV/Vis Spectrum

Methanol (analytical grade) from PanReac AppliChem (Castellar del Vallès, Barcelona, Spain) and lawsone from Acros Organics (Beel, Antwerp, Belgium) were used without further purification procedures. The absorption spectra of compounds in the methanolic solution were recorded using a Double Beam UV/VIS spectrophotometer Rayleigh—UV2601 (Beijing Beifen-Ruili Analytical Instrument, Beijing, China). A solvent blank was measured before each recorded spectrum. All measurements were performed at ambient temperature in standard quartz cuvettes of a 1 cm optical path.

3.4. Computational Calculations

The geometries of the studied compounds were optimized at the B3LYP, M06-2X, and HSE2PBE in addition to the 6-311+g(d,p) basis set. The electronic absorption spectra of the molecules in vacuum and methanol (MeOH) were simulated using time-dependent density functional theory (TD-DFT) at the B3LYP/6-311+G(d,p) level. The solvent effect was evaluated based on the polarizable continuum model (PCM) [46]. Calculations of the dyes attached to a cluster of $(\text{TiO}_2)_9$ were carried out following a known methodology [58,61] at DFT B3LYP with basis set 6-311G(d,p) for C, H, S, and O atoms, and LanL2DZ for Ti atoms. No imaginary vibrational frequencies were found at the optimized geometries, indicating that they are the true minima of the potential energy surface.

Density Functional Theory (DFT) and Time-Dependent Density Functional Theory (TD-DFT) calculations were performed using the Gaussian 09 (Gaussian, Inc., Wallingford, CT, USA) program package [47]. Natural Bond Orbital (NBO) calculations were carried out using NBOpro 6.0 (University of Wisconsin, Madison, WI, USA) program package [62]. All simulated absorption spectra were analyzed using GaussSum 3.0 [63].

4. Conclusions

The results of this study showed that, by linking lawsone with substituted benzenethiols, it is possible to obtain compounds exhibiting a gamma of colors with bathochromic shifts to a color close to red when compared with that of the parent compound. The inclusion of thiophenyl moiety in lawsone allows for absorption in a wide range of visible and UV wavelength range, compared with not substituted lawsone. Computational calculations employing Density Functional Theory (DFT) and Time-Dependent Density Functional Theory (TD-DFT) showed that the compounds presented lower excitation energies than lawsone, while the alignment of their frontier orbitals regarding the conduction bands of TiO_2 and ZnO and the redox potential of the electrolyte I^-/I_3^- suggests that they may be employed as sensitizers, like lawsone. Geometrical analysis showed that the incorporation of thiophenyl substituents on lawsone structure led to a loss of coplanarity, which favor an

anti-aggregation behavior, which is a factor that improves the open-circuit photovoltage (Voc) when dyes tend to form H-aggregation, as occur commonly in organic dyes with aromatic rings. The study of the interactions of the lawsone and 3-thiophenyl-lawsone with a TiO₂ surface model by different anchoring modes, showed that the absorption is thermodynamically favored. Natural bond orbital (NBO) analysis indicates a two-center bond (BD) O-Ti as the main interaction of the dyes with TiO₂, both in neutral and anionic state.

Supplementary Materials: The following are available online at <https://www.mdpi.com/article/10.3390/ma14195587/s1>, Table S1: Excitation energies (E_{ex}), wavelength (λ), oscillator strengths (f), light-harvesting efficiency (LHE), and the corresponding electronic transition for each relevant excited state, Table S2: Proposed assignation of experimental and calculated UV peak.

Author Contributions: Conceptualization, M.M.-C. (Maximiliano Martínez-Cifuentes) and R.A.-M.; methodology, M.M.-C. (Maximiliano Martínez-Cifuentes). O.F.-D.; validation, M.M.-C. (Maximiliano Martínez-Cifuentes), R.A.-M. and O.F.-D.; investigation, M.M.-C. (Matías Monroy-Cárdenas); data curation, M.M.-C. (Maximiliano Martínez-Cifuentes), O.F.-D. and M.M.-C. (Matías Monroy-Cárdenas); writing—original draft preparation, M.M.-C. (Maximiliano Martínez-Cifuentes), O.F.-D. and R.A.-M.; writing—review and editing, M.M.-C. (Maximiliano Martínez-Cifuentes) and R.A.-M.; visualization, M.M.-C. (Maximiliano Martínez-Cifuentes) and O.F.-D.; supervision, M.M.-C. (Maximiliano Martínez-Cifuentes) and R.A.-M.; project administration, M.M.-C. (Maximiliano Martínez-Cifuentes) and R.A.-M.; funding acquisition, M.M.-C. (Maximiliano Martínez-Cifuentes) and R.A.-M. All authors have read and agreed to the published version of the manuscript.

Funding: This research was funded by Fondo Nacional de Desarrollo Científico y Tecnológico (FONDECYT), grant No. 11170142 (Maximiliano Martínez-Cifuentes) and No. 1180069 (Ramiro Araya-Maturana).

Institutional Review Board Statement: Not applicable.

Informed Consent Statement: Not applicable.

Data Availability Statement: Data Sharing Not applicable.

Acknowledgments: Powered@NLHPC: this research was partially supported by the supercomputing infrastructure of the NLHPC (ECM-02).

Conflicts of Interest: The authors declare no conflict of interest.

References

1. Nguyen, M.V.C.; Lardy, B.; Rousset, F.; Hazane-Puch, F.; Zhang, L.; Trocme, C.; Serrander, L.; Krause, K.-H.; Morel, F. Quinone compounds regulate the level of ROS production by the NADPH oxidase Nox4. *Biochem. Pharmacol.* **2013**, *85*, 1644–1654. [[CrossRef](#)] [[PubMed](#)]
2. Song, Y.; Buettner, G.R. Thermodynamic and kinetic considerations for the reaction of semiquinone radicals to form superoxide and hydrogen peroxide. *Free Radic. Biol. Med.* **2010**, *49*, 919–962. [[CrossRef](#)] [[PubMed](#)]
3. Hillard, E.A.; de Abreu, F.C.; Ferreira, D.C.M.; Jaouen, G.; Goulart, M.O.F.; Amatore, C. Electrochemical parameters and techniques in drug development, with an emphasis on quinones and related compounds. *Chem. Commun.* **2008**, *23*, 2612–2628. [[CrossRef](#)]
4. Venil, C.K.; Velmurugan, P.; Dufossé, L.; Devi, P.R.; Ravi, A.V. Fungal Pigments: Potential coloring compounds for wide ranging applications in textile dyeing. *J. Fungi* **2020**, *6*, 68. [[CrossRef](#)] [[PubMed](#)]
5. Neta, P. Radiation chemistry of quinonoid compounds. *Quinonoid Compd.* **1988**, *2*, 879–898.
6. Martha, R.; Mubarak, M.; Darmawan, W.; Syafii, W.; Dumarcay, S.; Charbonnier, C.G.; Gérardin, P. Biomolecules of Interest Present in the Main Industrial Wood Species Used in Indonesia-A Review. *J. Renew. Mater.* **2021**, *9*, 399–449. [[CrossRef](#)]
7. Han, C.; Li, H.; Shi, R.; Zhang, T.; Tong, J.; Li, J.; Li, B. Organic quinones towards advanced electrochemical energy storage: Recent advances and challenges. *J. Mater. Chem. A* **2019**, *7*, 23378–23415. [[CrossRef](#)]
8. Bhuiyan, M.A.R.; Islam, A.; Islam, S.; Hossain, A.; Nahar, K. Improving dyeability and antibacterial activity of Lawsonia inermis L on jute fabrics by chitosan pretreatment. *Text. Cloth. Sustain.* **2017**, *3*, 1–10. [[CrossRef](#)]
9. Sauriasari, R.; Wang, D.-H.; Takemura, Y.; Tsutsui, K.; Masuoka, N.; Sano, K.; Horita, M.; Wang, B.-L.; Ogino, K. Cytotoxicity of lawsone and cytoprotective activity of antioxidants in catalase mutant Escherichia coli. *Toxicology* **2007**, *235*, 103–111. [[CrossRef](#)]
10. Mirza, S.; Akbar, Z.; Ahmad, M.S. A Simple Nondestructive, Cost-Effective Method for Differentiation of Protein Crystals from Salt Crystals by Using a Natural Dye. *Cryst. Growth Des.* **2019**, *19*, 3612–3615. [[CrossRef](#)]

11. Khadtare, S.S.; Ware, A.P.; Salunke-Gawali, S.; Jadkar, S.R.; Pingale, S.S.; Pathan, H.M. Dye sensitized solar cell with lawsone dye using a ZnO photoanode: Experimental and TD-DFT study. *RSC Adv.* **2015**, *5*, 17647–17652. [[CrossRef](#)]
12. Fantacci, S.; De Angelis, F. Ab initio modeling of solar cell dye sensitizers: The hunt for red photons continues. *Eur. J. Inorg. Chem.* **2019**, *2019*, 743–750. [[CrossRef](#)]
13. Kurpiers, J.; Ferron, T.; Roland, S.; Jakoby, M.; Thiede, T.; Jaiser, F.; Albrecht, S.; Janietz, S.; Collins, B.A.; Howard, I.A. Probing the pathways of free charge generation in organic bulk heterojunction solar cells. *Nat. Commun.* **2018**, *9*, 2038. [[CrossRef](#)] [[PubMed](#)]
14. Makoye, A.; Pogrebnoi, A.; Pogrebnyaya, T. Lawsone isomers, lawsone ether and bilawsone for dye-sensitized solar cells applications: DFT and UV-Vis studies. *J. Mol. Graph. Model.* **2020**, *94*, 107457. [[CrossRef](#)] [[PubMed](#)]
15. Chaiamornnugool, P.; Tontapha, S.; Phatchana, R.; Ratchapolthavisin, N.; Kanokmedhakul, S.; Sang-aroon, W.; Amornkitbamrung, V. Performance and stability of low-cost dye-sensitized solar cell based crude and pre-concentrated anthocyanins: Combined experimental and DFT/TDDFT study. *J. Mol. Struct.* **2017**, *1127*, 145–155. [[CrossRef](#)]
16. Sandquist, C.; McHale, J.L. Improved efficiency of betanin-based dye-sensitized solar cells. *J. Photochem. Photobiol. A Chem.* **2011**, *221*, 90–97. [[CrossRef](#)]
17. Ramamoorthy, R.; Radha, N.; Maheswari, G.; Anandan, S.; Manoharan, S.; Williams, R.V. Betalain and anthocyanin dye-sensitized solar cells. *J. Appl. Electrochem.* **2016**, *46*, 929–941. [[CrossRef](#)]
18. Orona-Navar, A.; Aguilar-Hernández, I.; Cerdán-Pasarán, A.; López-Luke, T.; Rodríguez-Delgado, M.; Cárdenas-Chávez, D.L.; Cepeda-Pérez, E.; Ornelas-Soto, N. Astaxanthin from *Haematococcus pluvialis* as a natural photosensitizer for dye-sensitized solar cell. *Algal Res.* **2017**, *26*, 15–24. [[CrossRef](#)]
19. Al-Alwani, M.A.; Ludin, N.A.; Mohamad, A.B.; Kadhum, A.A.H.; Sopian, K. Extraction, preparation and application of pigments from *Cordyline fruticosa* and *Hylocereus polyrhizus* as sensitizers for dye-sensitized solar cells. *Spectrochim. Acta Part A Mol. Biomol. Spectrosc.* **2017**, *179*, 23–31. [[CrossRef](#)]
20. Nan, H.; Shen, H.-P.; Wang, G.; Xie, S.-D.; Yang, G.-J.; Lin, H. Studies on the optical and photoelectric properties of anthocyanin and chlorophyll as natural co-sensitizers in dye sensitized solar cell. *Opt. Mater.* **2017**, *73*, 172–178. [[CrossRef](#)]
21. Brogdon, P.; Cheema, H.; Delcamp, J.H. Near-infrared-absorbing metal-free organic, porphyrin, and phthalocyanine sensitizers for panchromatic dye-sensitized solar cells. *ChemSusChem* **2018**, *11*, 86–103. [[CrossRef](#)] [[PubMed](#)]
22. Sreeja, S.; Pesala, B. Plasmonic enhancement of betanin-lawsone co-sensitized solar cells via tailored bimodal size distribution of silver nanoparticles. *Sci. Rep.* **2020**, *10*, 8240. [[CrossRef](#)] [[PubMed](#)]
23. Sreeja, S.; Pesala, B. Performance enhancement of betanin solar cells co-sensitized with indigo and lawsone: A Comparative Study. *ACS Omega* **2019**, *4*, 18023.
24. Bhuiyan, M.A.R.; Islam, A.; Ali, A.; Islam, M.N. Color and chemical constitution of natural dye henna (*Lawsonia inermis* L.) and its application in the coloration of textiles. *J. Clean. Prod.* **2017**, *167*, 14–22. [[CrossRef](#)]
25. Pallipurath, A.; Skelton, J.M.; Delori, A.; Duffy, C.; Erxleben, A.; Jones, W. Crystalline adducts of the Lawsone molecule (2-hydroxy-1,4-naphthaquinone): Optical properties and computational modelling. *CrystEngComm* **2015**, *17*, 7684–7692. [[CrossRef](#)]
26. Monroy-Cárdenas, M.; Méndez, D.; Trostchansky, A.; Martínez-Cifuentes, M.; Araya-Maturana, R.; Fuentes, E. Synthesis and Biological Evaluation of Thio-Derivatives of 2-Hydroxy-1, 4-Naphthoquinone (Lawsone) as Novel Antiplatelet Agents. *Front. Chem.* **2020**, *8*, 533. [[CrossRef](#)] [[PubMed](#)]
27. Alebeid, O.K.; Pei, L.; Elhassan, A.; Zhou, W.; Wang, J. Cleaner dyeing and antibacterial activity of wool fabric using Henna dye modified with *Acacia nilotica* pods. *Clean Technol. Environ. Policy* **2020**, *22*, 2223–2230. [[CrossRef](#)]
28. Räsänen, R.; Nousiainen, P.; Hynninen, P.H. Emodin and dermocybin natural anthraquinones as high-temperature disperse dyes for polyester and polyamide. *Text. Res. J.* **2001**, *71*, 922–927. [[CrossRef](#)]
29. Patil, S.R.; Choudhary, A.S.; Sekar, N. Disperse styryl and azo dyes for polyester and nylon fibre: Synthesis, optical properties having the 1, 2, 4-triketone naphthoquinone skeleton. *Fibers Polym.* **2015**, *16*, 1068–1074. [[CrossRef](#)]
30. Kathawate, L.; Joshi, P.V.; Dash, T.K.; Pal, S.; Nikalje, M.; Weyhermüller, T.; Puranik, V.G.; Konkimalla, V.B.; Salunke-Gawali, S. Reaction between lawsone and aminophenol derivatives: Synthesis, characterization, molecular structures and antiproliferative activity. *J. Mol. Struct.* **2014**, *1075*, 397–405. [[CrossRef](#)]
31. Mahkam, M.; Kafshboran, H.R.; Nabati, M. Synthesis and characterization of novel colored polymers based on lawsone natural compound. *Des. Monomers Polym.* **2014**, *17*, 784–794. [[CrossRef](#)]
32. Zollinger, H. *Color Chemistry: Syntheses, Properties, and Applications of Organic Dyes and Pigments*; John Wiley & Sons: Hoboken, NJ, USA, 2003; ISBN 3906390233.
33. Chandrakalavathi, T.; Sudha, V.; Sindhuja, M.; Harinipriya, S.; Jeyalakshmi, R. Photosonelectrochemical analysis of *Lawsonia inermis* (henna) and artificial dye used in tattoo and dye industry. *J. Photochem. Photobiol. A Chem.* **2018**, *360*, 44–57. [[CrossRef](#)]
34. Dhaouadi, K.; Meliti, W.; Dallali, S.; Belkhir, M.; Ouerghemmi, S.; Sebei, H.; Fattouch, S. Commercial *Lawsonia inermis* L. dried leaves and processed powder: Phytochemical composition, antioxidant, antibacterial, and allelopathic activities. *Ind. Crops Prod.* **2015**, *77*, 544–552. [[CrossRef](#)]
35. Kavitha, S.; Praveena, K.; Lakshmi, M. A new method to evaluate the feasibility of a dye in DSSC application. *Int. J. Energy Res.* **2017**, *41*, 2173–2183.
36. Ouared, I.; Rekis, M.; Trari, M. Phenothiazine based organic dyes for dye sensitized solar cells: A theoretical study on the role of π -spacer. *Dye. Pigment.* **2021**, *190*, 109330. [[CrossRef](#)]
37. Zhang, L.; Cole, J.M. Dye aggregation in dye-sensitized solar cells. *J. Mater. Chem. A* **2017**, *5*, 19541–19559. [[CrossRef](#)]

38. Choi, H.; Baik, C.; Kang, S.O.; Ko, J.; Kang, M.; Nazeeruddin, M.K.; Grätzel, M. Highly efficient and thermally stable organic sensitizers for solvent-free dye-sensitized solar cells. *Angew. Chem.* **2008**, *120*, 333–336. [[CrossRef](#)]
39. Ooyama, Y.; Harima, Y. Photophysical and electrochemical properties, and molecular structures of organic dyes for dye-sensitized solar cells. *ChemPhysChem* **2012**, *13*, 4032–4080. [[CrossRef](#)]
40. Kalyanasundaram, K. *Dye-Sensitized Solar Cells*; CRC press: Boca Raton, FL, USA, 2010; ISBN 143980866X.
41. Ghamdi, S.N.A.L.; Ghamdi, H.A.A.L.; El-Shishtawy, R.M.; Asiri, A.M. Advances in phenothiazine and phenoxazine-based electron donors for organic dye-sensitized solar cells. *Dye. Pigment.* **2021**, *194*, 109638. [[CrossRef](#)]
42. Lu, Y.; Song, H.; Li, X.; Ågren, H.; Liu, Q.; Zhang, J.; Zhang, X.; Xie, Y. Multiply wrapped porphyrin dyes with a phenothiazine donor: A high efficiency of 11.7% achieved through a synergetic coadsorption and cosensitization approach. *ACS Appl. Mater. Interfaces* **2019**, *11*, 5046–5054. [[CrossRef](#)]
43. Zhao, D.; Lu, Q.; Su, R.; Li, Y.; Zhao, M. Light harvesting and optical-electronic properties of two quercetin and rutin natural dyes. *Appl. Sci.* **2019**, *9*, 2567. [[CrossRef](#)]
44. Sun, C.; Li, Y.; Song, P.; Ma, F. An experimental and theoretical investigation of the electronic structures and photoelectrical properties of ethyl red and carminic acid for DSSC application. *Materials* **2016**, *9*, 813. [[CrossRef](#)] [[PubMed](#)]
45. Madili, N.; Pogrebnoi, A.; Pogrebnya, T. Theoretical design of complex molecule via combination of natural lawsone and synthetic indoline D131 dyes for dye sensitized solar cells application. *Comput. Chem.* **2018**, *6*, 87. [[CrossRef](#)]
46. Oprea, C.I.; Frecuș, B.; Minaev, B.F.; Gîrțu, M.A. DFT study of electronic structure and optical properties of some Ru- and Rh-based complexes for dye-sensitized solar cells. *Mol. Phys.* **2011**, *109*, 2511–2523. [[CrossRef](#)]
47. Li, Y.; Liu, J.; Liu, D.; Li, X.; Xu, Y. DA- π -A based organic dyes for efficient DSSCs: A theoretical study on the role of π -spacer. *Comput. Mater. Sci.* **2019**, *161*, 163–176. [[CrossRef](#)]
48. Fujisawa, J.; Eda, T.; Hanaya, M. Comparative study of conduction-band and valence-band edges of TiO₂, SrTiO₃, and BaTiO₃ by ionization potential measurements. *Chem. Phys. Lett.* **2017**, *685*, 23–26. [[CrossRef](#)]
49. Jose, R.; Thavasi, V.; Ramakrishna, S. Metal oxides for dye-sensitized solar cells. *J. Am. Ceram. Soc.* **2009**, *92*, 289–301. [[CrossRef](#)]
50. Sang-aroon, W.; Saekow, S.; Amornkitbamrung, V. Density functional theory study on the electronic structure of Monascus dyes as photosensitizer for dye-sensitized solar cells. *J. Photochem. Photobiol. A Chem.* **2012**, *236*, 35–40. [[CrossRef](#)]
51. Prinzişky, C.; Meyenburg, I.; Jacob, A.; Heidelmeier, B.; Schröder, F.; Heimbrod, W.; Sundermeyer, J. Optical and Electrochemical Properties of Anthraquinone Imine Based Dyes for Dye-Sensitized Solar Cells. *Eur. J. Org. Chem.* **2016**, *2016*, 756–767. [[CrossRef](#)]
52. Sánchez-de-Armas, R.; Oviedo Lopez, J.A.; San-Miguel, M.; Sanz, J.F.; Ordejón, P.; Pruneda, M. Real-time TD-DFT simulations in dye sensitized solar cells: The electronic absorption spectrum of alizarin supported on TiO₂ nanoclusters. *J. Chem. Theory Comput.* **2010**, *6*, 2856–2865. [[CrossRef](#)]
53. Sánchez-de-Armas, R.; Oviedo, J.; San Miguel, M.Á.; Sanz, J.F. Direct vs indirect mechanisms for electron injection in dye-sensitized solar cells. *J. Phys. Chem. C* **2011**, *115*, 11293–11301. [[CrossRef](#)]
54. Zhang, J.; Zhu, H.-C.; Zhong, R.-L.; Wang, L.; Su, Z.-M. Promising heterocyclic anchoring groups with superior adsorption stability and improved IPCE for high-efficiency noncarboxyl dye sensitized solar cells: A theoretical study. *Org. Electron.* **2018**, *54*, 104–113. [[CrossRef](#)]
55. Li, Y.; Song, P.; Yang, Y.; Ma, F.; Li, Y. Double-anchoring organic dyes for dye-sensitized solar cells: The opto-electronic property and performance. *New J. Chem.* **2017**, *41*, 12808–12829. [[CrossRef](#)]
56. Urzúa-Leiva, R.; Pino-Rios, R.; Cárdenas-Jirón, G. The influence of antenna and anchoring moieties on the improvement of photoelectronic properties in Zn (ii)-porphyrin-TiO₂ as potential dye-sensitized solar cells. *Phys. Chem. Chem. Phys.* **2019**, *21*, 4339–4348. [[CrossRef](#)]
57. Slimi, A.; Hachi, M.; Fitri, A.; Benjelloun, A.T.; Elkhatabi, S.; Benzakour, M.; Mcharfi, M.; Khenfouch, M.; Zorkani, I.; Bouachrine, M. Effects of electron acceptor groups on triphenylamine-based dyes for dye-sensitized solar cells: Theoretical investigation. *J. Photochem. Photobiol. A Chem.* **2020**, *398*, 112572. [[CrossRef](#)]
58. Fadili, D.; Bouzzine, S.M.; Hamidi, M. Study of the structural and optoelectronic properties of dye solar cells based on phosphonic acid anchoring by DFT functionals. *New J. Chem.* **2021**, *45*, 2723–2733. [[CrossRef](#)]
59. Tian, H.; Yang, X.; Chen, R.; Zhang, R.; Hagfeldt, A.; Sun, L. Effect of different dye baths and dye-structures on the performance of dye-sensitized solar cells based on triphenylamine dyes. *J. Phys. Chem. C* **2008**, *112*, 11023–11033. [[CrossRef](#)]
60. Frenking, G.; Shaik, S. *The Chemical Bond: Fundamental Aspects of Chemical Bonding*; John Wiley & Sons: Hoboken, NJ, USA, 2014; ISBN 3527664718.
61. Oprea, C.I.; Gîrțu, M.A. Structure and electronic properties of TiO₂ nanoclusters and dye-nanocluster systems appropriate to model hybrid photovoltaic or photocatalytic applications. *Nanomaterials* **2019**, *9*, 357. [[CrossRef](#)] [[PubMed](#)]
62. Glendening, E.D.; Badenhop, J.K.; Reed, A.E.; Carpenter, J.E.; Bohmann, J.A.; Morales, C.M.; Landis, C.R.; Weinhold, F. *NBO v. 6.0. Program*; University of Wisconsin: Madison, WI, USA, 2013.
63. O'boyle, N.M.; Tenderholt, A.L.; Langner, K.M. Cclib: A library for package-independent computational chemistry algorithms. *J. Comput. Chem.* **2008**, *29*, 839–845. [[CrossRef](#)] [[PubMed](#)]